Multiparametric assessment of cellular lipid metabolism in hypercholesterolemia

Simon G. Pfisterer[1]*, PhD, Ivonne Brock[1,2,3], PhD, Kristiina Kanerva[1,2,3], PhD, Iryna Hlushchenko[1], PhD, Lassi Paavolainen[4], PhD, Pietari Ripatti[4], MD, Mohammad M. Islam[1], Aija Kyttälä[5], PhD, Maria D. Di Taranto[6,7], PhD, Annalisa Scotto di Frega[7], Giuliana Fortunato[6,7], MD, Johanna Kuusisto[8], MD, Peter Horvath[4,9], PhD, Samuli Ripatti[4,10,11], PhD, Markku Laakso[8], MD PhD, Elina Ikonen[1,2,3]*, MD PhD

Affiliations:

1) Department of Anatomy, Faculty of Medicine, University of Helsinki, Helsinki, Finland; **2**) Stem Cells and Metabolism Research Program, Faculty of Medicine, University of Helsinki, Helsinki, Finland; **3**) Minerva Foundation Institute for Medical Research, Helsinki, Finland; **4**) Institute for Molecular Medicine Finland (FIMM), HiLIFE, University of Helsinki, Helsinki, Finland; **5**) Finnish Institute for Health and Welfare (THL), THL Biobank, Helsinki, Finland; **6**) Department of Molecular Medicine and Medical Biotechnologies, University of Naples Federico II, Italy; **7)** CEINGE Biotecnologie Avanzate scarl Naples, Italy; **8**) Department of Medicine, University of Eastern Finland and Kuopio University Hospital, Kuopio, Finland; **9**) Biological Research Center, Szeged, Hungary; **10)** Department of Public Health, Clinicum, Faculty of Medicine, University of Helsinki, Helsinki, Finland; **11)** The Broad Institute of MIT and Harvard, Cambridge, MA, USA, *corresponding authors.

Abstract:

Differences in cellular lipid metabolism may underlie large interindividual variability in lipid disorders such as hypercholesterolemia. Here, we established a multi-parametric imaging platform enabling the quantification of lipid uptake and storage in cytoplasmic droplets of leukocyte populations from 2-4 ml of peripheral blood. We define a new quantifiable parameter, cellular lipid mobilization, describing the efficiency at which cells deplete their lipid reservoirs. The 65 individuals studied, including heterozygous familial hypercholesterolemia (He-FH) patients with identical LDL receptor mutations, showed distinct profiles of low-density lipoprotein (LDL) uptake and lipid mobilization. Lipid mobilization correlated positively with cellular LDL uptake and negatively with hypercholesterolemia, increased body mass index and age. Lipid mobilization and LDL uptake distinguished good and poor statin responders among He-FH patients, and their combination with polygenic scores improved the risk assessment in hypercholesterolemia within a general population subcohort. Together, these findings open up new avenues for personalized medicine approaches in hypercholesterolemia.

Introduction:

Hypercholesterolemia is a major risk factor for cardiovascular disease (CVD) and one of the most common metabolic disorders. It is characterized by an accumulation of low-density lipoprotein (LDL) cholesterol (LDL-c) in the blood[1]. In familial hypercholesterolemia (FH), mutations, most commonly in the LDL receptor (*LDLR*) gene, lead to increased LDL-c. However, FH represents only 2.5% of all hypercholesterolemia patients. For the remainder, polygenic and lifestyle effects appear as the main contributing factors[2-5].

Several pharmacological treatments are available for hypercholesterolemia, enabling efficient LDL-c lowering. These include statins, ezetimibe, PCSK9 inhibitors and their combinations[6]. Statins are the first line medication, but more than 30% of statin-recipients do not respond to it well, requiring additional treatments[7,8]. Moreover, most high-risk hypercholesterolemia patients do not achieve their LDL-c target levels, leaving them at increased risk for CVD[9]. This highlights the need for better patient stratification tools in hypercholesterolemia. Cell-based assays are increasingly used for personalized treatment decisions in cancer therapy[10], but are not developed to a similar degree in the management of hypercholesterolemia.

Several studies, mostly based on radioactive LDL, have shown that low cellular LDL uptake correlates with high circulating LDL-c in heterozygous FH patients receiving statins[11,12]. However, it has been challenging to demonstrate similar effects with non-radioactive assays due to lower sensitivity[13]. Fluorescent LDL uptake studies have been carried out in different cell types such as lymphocytes, monocytes and Epstein-Barr virus (EBV) immortalized lymphoblasts[14,15]. EBV lymphoblasts show the highest LDL uptake, but the immortalization of cells is time consuming and alters their functions[14,16]. Currently, quantification of cellular LDL

uptake is performed in specialized research laboratories to characterize the severity of LDLR mutations in FH patients[17,18], but it has not reached wider utility for patient treatment or risk stratification.

LDLR expression and cellular LDL internalization are tightly regulated. Low cholesterol levels in the endoplasmic reticulum (ER) signal cholesterol starvation and trigger increased LDLR expression, while high cholesterol in the ER downregulates LDLR expression. Excess cholesterol and fatty acids are stored in lipid droplets (LD) connected to the ER, from where they can be mobilized upon need[19,20]. We therefore considered that quantification of cellular LDs and their dynamic changes may provide additional information for assessing the cellular basis of hypercholesterolemia.

Here, we established sensitive and scalable analyses for automated quantification of fluorescent lipid uptake and storage in primary lymphocyte and monocyte populations, and defined lipid mobilization as a novel parameter measuring how efficiently cells deplete their lipid stores. We found that individuals, including He-FH patients with identical LDLR mutations, showed marked differences in lipid uptake, storage and mobilization. Lipid mobilization was lower in persons with hypercholesterolemia, increased body mass index (BMI) or age. Finally, we demonstrate the potential of lipid uptake and mobilization scores in distinguishing responsiveness to statin therapy and in improving risk assessment in hypercholesterolemia.

Results:

Automated pipeline for multiplex quantification of hypercholesterolemia-related functional defects in primary human leukocytes

We set up an automated imaging and analysis pipeline to quantify LDL uptake, LDLR surface expression and lipid storage under different conditions from less than two million peripheral blood mononuclear cells (PBMCs) (2-4 ml blood) (**Fig. 1a**). Cryopreserved PBMCs were recovered in 96 well plates at defined densities and incubated with lipid-rich control medium (CM, 10% FBS) or lipid poor medium (LP, 5% lipoprotein-deficient serum) for 24 h. Cells were labelled with fluorescent LDL particles (DiI-LDL) for 1 h, washed and automatically transferred to 384 well plates for staining and automated high-content imaging (**Fig. 1a**). After adhesion to coated imaging plates, lymphocytes remain small while monocytes spread out, enabling identification of leukocyte populations based on size: PBMCs with a cytoplasmic area <115 μm^2 were classified as lymphocytes and those with a cytoplasmic area >115 μm^2 as monocytes (**Extended Data Fig. 1 a-c**).

In CM, DiI-LDL uptake into lymphocytes and monocytes was more than two-fold above the background of non-labeled cells (**Fig. 1b-d**). Lipid starvation further increased DiI-LDL uptake in both cell populations (**Fig. 1c, d**). We aggregated the single-cell data from individual wells and averaged the results from 2-4 wells for each treatment, enabling the quantification of about 700 monocytes and 2300 lymphocytes per well (**Extended Data Fig. 1d**). For both cell populations, we defined two readouts, cellular DiI-LDL intensity (DiI-Int), reflecting DiI-LDL surface binding and internalization, and DiI-LDL organelle number (DiI-No), reflecting internalized DiI-LDL (**Fig 1e, f**). This results in four parameters: monocyte (Mo) DiI-Int,

lymphocyte (Ly) DiI-Int, Mo DiI-No and Ly DiI-No. In both cell populations, DiI-Int was inhibited by adding surplus unlabeled LDL, arguing for a saturable, receptor-mediated uptake mechanism (**Extended Data Fig. 1e**).

In lipid rich conditions, Mo DiI-Int was slightly higher than Ly DiI-Int (**Fig. 1e**), and upon lipid starvation, Mo DiI-Int increased more profoundly, providing a larger fold increase than Ly DiI-Int (**Fig. 1e**). Furthermore, Mo DiI-No was roughly ten-fold higher than Ly DiI-No, with both parameters showing a five-fold increase upon lipid starvation (**Fig. 1f**). Thus, DiI-LDL uptake into monocytes is better than into lymphocytes, but both cell populations respond to lipid starvation. EBV lymphoblasts are often a preferred choice for LDL uptake studies[20]. We therefore compared LDL uptake in EBV lymphoblasts and monocytes (**Extended Data Fig. 1f,g**). This showed that DiI-Int signal intensity after lipid starvation was roughly similar in EBV-lymphoblasts and monocytes, implying that the primary cells provide high enough DiI-LDL signal intensities without time consuming cell immortalization (**Extended Data Fig. 1g**).

To enable data comparison between the experiments, we included two controls. Each control consisted of a mixture of large-scale PBMC isolations from four healthy blood donors, with the cells cryopreserved at a defined density for one-time use aliquots. In each experiment, Mo DiI-Int, Ly DiI-Int, Mo DiI-No and Ly DiI-No were normalized to these controls. We also introduced a combinatorial score, pan-LDL uptake (or pan-uptake), representing the average of Mo DiI-Int, Ly DiI-Int, Mo DiI-No and Ly DiI-No. We then assessed the intraindividual variability of these five readouts in three individuals on two consecutive days (**Extended Data Fig. 1h**). The intraindividual variability was low for a cell-based assay, especially in monocytes, with 7.6% for

Mo DiI-No, 12% for Mo DiI-Int and 13% for pan-uptake. The values were only moderately higher in lymphocytes, with DiI-Int 15% and DiI-No 21.1% (**Extended Data Fig. 1i**).

We next validated our LDL uptake measurements in PBMCs of two He-FH patients (Cys325Tyr and Ser580Phe mutations in *LDLR*) with highly elevated LDL-c, and reduced LDL uptake in EBV lymphoblasts (**Extended Data Fig. 1j**). For both patients, Mo and Ly DiI-No as well as Mo DiI-Int were reduced by more than 45%, Ly DiI-Int was less profoundly decreased, and pan-uptake was reduced by over 50% (**Fig. 1g, h; Extended Data Fig. 1j**). Together, these data indicate that our analysis pipeline enables quantification of multiple LDL uptake parameters in major leukocyte cell populations and distinguishes defective LDLR function therein.

Heterogeneous LDL uptake and LDLR surface expression in He-FH patients with identical LDLR mutations

We next used our analysis pipeline to characterize 21 He-FH patients from the Metabolic Syndrome in Men (METSIM) cohort study[21] (**Extended Data Table 1**). The patients' mutations are localized in the *LDLR* coding region, ranging from pathogenic to likely benign variants (**Fig. 2a**). Quantification of DiI-Int and DiI-No for monocytes and lymphocytes provided highly similar results for each person (**Fig. 2b**). However, there were substantial interindividual differences for the LDL uptake parameters, also between persons harboring identical *LDLR* mutations (**Fig. 2b**). This was most pronounced for FH-North Karelia (Pro309Lysfs*59), a pathogenic loss of function variant, but also evident for FH-Pogosta (Arg595Gln) and FH-Glu626Lys (**Fig. 2a, b**). These observations suggest that in He-FH, regulatory mechanisms may

enhance the expression of the unaffected *LDLR* allele and/or stabilize the encoded protein. In support, we obtained a strong correlation between monocyte LDLR surface expression and DiI-Int, DiI-No and pan-uptake scores for the same individuals (pan-uptake, R=0.58, p=0.006), (**Fig. 2c, Extended Data Fig. 2a**).

Interestingly, the pan-uptake score showed a tendency for lower values in FH-North Karelia variants as compared to the likely pathogenic FH-Pogosta and likely benign Glu626Lys variants (**Extended Data Fig. 2b**). This is in agreement with higher LDL-c concentrations in FH-North Karelia patients[22]. While LDL uptake did not correlate with circulating LDL-c for all FH patients (**Extended Data Fig. 2c**), for He-FH patients on statin monotherapy, this correlation was highly significant for monocyte DiI-Int, DiI-No and the pan-uptake scores (Mo DiI-Int: R=-0.75, p=0.0081, **Fig. 2d**). Importantly, 30% of the individuals with the lowest monocyte DiI-Int had a two-fold higher LDL-c concentration than the 30% with the highest monocyte DiI-Int (**Fig. 2e**). We therefore classified these two patient groups as good and poor statin responders (**Fig. 2e**).

LDL uptake in non-FH individuals with normal or elevated blood LDL-c

Most hypercholesterolemia patients do not carry LDLR mutations[2]. We therefore investigated cellular LDL uptake in PBMCs from 20 biobank donors with elevated LDL-c levels (LDL-c >5 mM) (hLDL-c) and from 19 donors with normal LDL levels (LDL-c 2-2.5 mM) (nLDL-c) from the FINRISK population cohort[23] (**Extended Data Table 2**). DNA sequencing confirmed that common Finnish *LDLR* variants were not present among these subjects.

We quantified DiI-Int and DiI-No for monocyte and lymphocyte populations as well as the pan-uptake score for nLDL-c and hLDL-c individuals. This revealed a large interindividual variability in LDL uptake (**Fig. 3a**). Both groups included persons with severely reduced LDL internalization, but the lowest pan-LDL uptake scores were in the hLDL-c individuals (**Fig. 3a**). Overall, pan-uptake and Ly DiI-No were reduced in hLDL-c compared to nLDL-c subjects, but the differences were not significant (**Extended Data Fig. 3a, b**). Of note, reduced pan-uptake, Mo DiI-Int and Ly DiI-No correlated with increased blood LDL-c levels in the hLDL-c subgroup, but the correlations relied on a single individual with a very high blood LDL-c concentration (**Extended Data Fig. 3c**).

To investigate additional factors influencing the interindividual variability in cellular LDL uptake, we analyzed correlations to two obesity indicators, body mass index (BMI) and waist circumference. Strikingly, reduced pan-uptake, as well as Mo DiI-Int, and Ly DiI-Int correlated with increased waist circumference (pan-uptake: R=-0.42, p=0.009; **Fig. 3b**). Lower pan-uptake, Ly DiI-Int and Mo DiI-Int also correlated with elevated BMI (pan-uptake: R=-0.36, p=0.022; **Fig. 3 c**).

Assessment of cellular lipid storage and mobilization in leukocytes

Cells store excess lipids in LDs and this is related to lipid uptake: When peripheral cells have sufficient lipids available, they typically exhibit LDs and in parallel, lipid uptake is downregulated. Staining of PBMCs in lipid rich conditions (CM) with the LD dye LD540 revealed that lymphocytes and monocytes displayed LDs in a heterogenous fashion (**Fig. 4a**),

with lymphocytes showing fewer LD positive cells and fewer LDs per cell than monocytes (**Fig. 4b, c**). We then visualized the changes in LD abundance upon overnight lipid starvation (LP) (**Fig. 4b-f**). This resulted in a pronounced decrease in lipid deposition: In CM, 9% of lymphocytes and 25% of monocytes contained LDs, but upon lipid starvation, these were reduced to 6% (Ly) and 12% (Mo) (**Fig. 4d**).

Due to the lower LD abundance in lymphocytes, we focused on monocytes and defined three readouts for them: 1) Percentage of LD-positive cells (LD-Pos), 2) Cellular LD number in LD-Pos (LD-No) and 3) Total cellular LD Area in LD-Pos (LD-Area). On average, LD-Pos cells showed 2.9 LDs in lipid rich conditions and 1.8 LDs upon lipid starvation (**Fig. 4e**). The total LD area decreased from 1.35 μm^2 in lipid rich conditions to 0.8 μm^2 upon lipid starvation (**Fig. 4f**).

When quantifying LD parameters from several subjects, we observed substantial differences between individuals in how LDs changed upon lipid starvation. To systematically quantify these differences, we established a parameter, lipid mobilization score, that reflects how efficiently cellular lipid stores are depleted under lipid starvation (**Fig. 4g**). Lipid mobilization scores were calculated for each of the LD readouts, LD-Pos, LD-No and LD-Area, by dividing the results obtained in lipid rich conditions with those obtained after lipid starvation (**Fig. 4g**). Furthermore, we established a pan-mobilization score by averaging LD-Pos, LD-No and LD-Area scores (**Fig. 4g, h**), with LD-Pos providing the highest mobilization score but also the highest variability (**Fig. 4h**).

To further assess the reliability of the LD mobilization parameters, we determined their intraindividual variation using the same samples as for analyzing intraindividual variation of DiI-LDL uptake (**Extended Data Fig. 1i, j**). This showed a modest intraindividual variation for the

lipid mobilization scores (**Extended Data Fig. 4a**), which was on average 8% for pan-mobilization, 10% for LD-Pos, 11% for LD-No and 13% for LD-Area (**Extended Data Fig. 4b**).

Cellular lipid mobilization in He-FH patients

When lipid mobilization was analyzed from the He-FH samples of the METSIM cohort, we found that the pan-mobilization score was significantly reduced in He-FH individuals carrying the FH-North Karelia and Glu626Lys variants (**Fig. 4i**). This suggests that defective LDLR function may be accompanied by reduced lipid mobilization. We also studied whether the combination of a lipid mobilization score with LDL uptake improves the stratification of He-FH patients with respect to their statin responsiveness. Several of the patients showed low monocyte DiI-LDL intensities in a narrow range (**Fig. 2d**). When monocyte DiI-Int was combined with the pan- mobilization score, larger differences between patients were observed, providing a better separation between high LDL-c (poor statin responders) and intermediate LDL-c patients (**Fig. 4j**). Moreover, the difference in LDL-c concentration between good and poor statin responders was more significant when using the combined lipid uptake and mobilization scores than when using monocyte DiI-Int alone (**Fig. 4k vs. Fig. 2e**).

Cellular lipid mobilization is reduced in non-FH hypercholesterolemia patients and correlates with LDL uptake

We then investigated whether monocytes from nLDL-c and hLDL-c biobank donors displayed differences in lipid mobilization. Analogously to LDL uptake, we observed a large variability for

the pan- and individual mobilization scores in this cohort (**Fig. 5a**). Interestingly, pan-mobilization, LD-No and LD-Area were significantly reduced in the hLDL-c compared to nLDL-c subjects (**Fig. 5a, b, Extended Data Fig. 5a, b**). This prompted us to scrutinize whether lipid mobilization correlates with LDL uptake related parameters or obesity indicators in this cohort. All mobilization scores correlated positively with the pan-uptake score (R=0.42, p=0.0095 for pan-mobilization; **Fig. 5c**). Furthermore, pan-, LD-No and LD-Area mobilization scores correlated negatively with total cholesterol and apo-B concentrations (**Extended Data Fig. 5c, d**). Remarkably, the pan-mobilization score correlated negatively with BMI (R=-0.34, p=0.036; **Fig. 5d**) and LD-No, and LD-Area were negatively correlated with waist circumference (R=-0.32, p=0.0495 for LD-No; **Extended Data Fig. 5e)**. Moreover, higher LD-No, LD-Area and pan-mobilization scores correlated negatively with age (R=-0.38, p=0.019 for pan-mobilization; **Fig. 5e**.

Hybrid scores of genetic and functional cell data improve risk assessment in hypercholesterolemia

The hLDL-c biobank donors of the FINRISK population cohort displayed an increased LDL-polygenic risk score (LDL-PRS) (**Fig. 6a**). Of note, LDL-PRS did not correlate with LDL uptake or lipid mobilization (**Extended Data Fig. 6a, b**), suggesting that LDL-PRS and cellular LDL uptake monitor at least in part distinct processes. Interestingly, combination of LDL-PRS with pan-uptake reduced the variation and made it easier to discriminate nLDL-c and hLDL-c populations, providing an eight times better p-value as compared to LDL-PRS only (**Fig. 6b**). Furthermore, combination of the pan-mobilization score with LDL-PRS drastically improved the

discrimination of both groups (**Fig. 6c**) and combining all three parameters, i.e. LDL-PRS, pan-uptake and pan-mobilization, provided the best discrimination power and lowest p-value, 60-fold better than LDL-PRS alone (**Fig. 6d**). To estimate the association of LDL-PRS and novel hybrid scores with elevated LDL-c (>5 mmmol/l), we calculated the odds ratio (OR) for elevated LDLc by comparing individuals with the highest 30% of the score to the remaining subjects. Combining LDL-PRS either with pan-uptake or pan-mobilization doubled the OR and using the hybrid score combining all three readouts resulted in a five-fold higher OR (**Fig. 6e**).

Conclusions:

In this study, we established a multiplexed high-content analysis pipeline to quantify lipid uptake and storage in primary lymphocyte and monocyte populations, analyzing over 310 conditions (combinations of assays and treatments) from 65 patient samples. Overall, besides automation of cell handling, staining and imaging procedures enabling high-throughput applications, this platform provides significant advantages over existing methodologies to assess the lipid status in PBMCs: Immobilization of cells to coated surfaces allows image acquisition after sample storage and subcellular imaging resolution enables quantification of internalized LDL as well as LDs.

So far only a single readout, LDL uptake, has been used to gain insight into the cellular mechanisms underlying hypercholesterolemia in human subjects. Somewhat unexpectedly, we observed highly divergent LDL uptake and LDLR surface expression patterns even for FH individuals carrying identical *LDLR* mutations. This argues that the *LDLR* genotype is not a uniformly dominant determinant of cellular LDL uptake. Furthermore, the LDL uptake readouts

enabled us to demonstrate a correlation of high LDL uptake with low circulating LDL-c for He-FH patients on statin treatment. Pending validation in bigger patient groups, this suggests that our analyses may help to determine good and poor statin responders in He-FH patients. Of note, monocytes appear superior to lymphocytes for evaluating a person's statin responsiveness, most probably due to higher LDL uptake that yields larger interindividual differences.

We also found marked differences in cellular LDL uptake in individuals who did not carry common Finnish FH mutations, irrespective of their LDL-c levels. This prompted us to search for additional imaging-based readouts to compare lipid handling between individuals and to better explain the variation in LDL-c in the population. To this end, we analyzed lipid storage in droplets and their consumption during starvation and established a new parameter, lipid mobilization score, that quantifies the changes in LD-related parameters between lipid-rich and -poor conditions.

Interestingly, large differences between individuals were also characteristic to cellular lipid storage and utilization. Increased lipid mobilization correlated with increased LDL uptake, implying that efficient removal of cellular lipids is typically paralleled by efficient lipid uptake. Importantly, in the FINRISK population cohort, lipid mobilization outperformed LDL uptake in distinguishing individuals with high LDL-c (>5 mmol/l) and low LDL-c (2-2.5 mmol/l). Furthermore, by combining LDL uptake and lipid mobilization parameters for He-FH patients on statin therapy, it was easier to pinpoint individuals with an insufficient statin response. Therefore, lipid mobilization emerges as a useful parameter with potential for improving patient stratification and risk assessment in hypercholesterolemia.

Obesity is typically linked to dyslipidemia characterized by decreased high-density lipoprotein cholesterol (HDL-c), increased small dense LDL particles and elevated LDL-c. This profile is often attributed to defective lipolysis of TG-rich lipoproteins[24]. We found that increased BMI and waist circumference correlated with reduced LDL uptake and lipid mobilization. These results suggest that defective LDL clearance may contribute to dyslipidemia in obesity, with reduced lipid mobilization potentially underlying decreased LDL uptake. Accordingly, LDLR expression has been reported to be reduced in obesity[25].

Polygenic risk scores (PRS) provide novel tools for personalized risk assessment and are increasingly included in clinical care guidelines of hypercholesterolemia[1,6]. Hypercholesterolemic subjects of the FINRISK cohort showed an increased LDL-PRS, but this did not correlate with LDL uptake or lipid mobilization, arguing that the cell functional parameters cover in part different territories than PRS. We therefore investigated if combining LDL-PRS and cell-based data improves hypercholesterolemia risk assessment. Indeed, the combination of LDL uptake, lipid mobilization and LDL-PRS drastically improved the segregation of hyper- and normocholesterolemic subjects, with a 60-fold improved p-value and a 5-fold higher OR as compared to LDL-PRS alone. We envisage that in the future, such hybrid scores may facilitate the detection of hypercholesterolemia risk at young age when clinical CVD manifestations are not yet overt, thus enabling faster initiation of treatment and improved disease prevention[26].

In summary, this study establishes novel automated assays for reliable quantification of lipid uptake and mobilization in human leukocytes, providing unprecedented insights into the cellular mechanisms underlying hypercholesterolemia. These readouts are expected to facilitate

personalized medicine approaches in hypercholesterolemia, as exemplified by the possibility to identify individuals with an unsatisfactory statin response, for potential co-treatment with ezetimibe/PCSK9 inhibitors, and to significantly improve risk assessment in hypercholesterolemia and CVD from that obtained with PRS alone.

Methods:

Materials: Lipoprotein deficient serum (LPDS) was obtained from fetal bovine serum by ultracentrifugation as described[27]. For DiI-LDL, we first prepared fresh LDL from human plasma samples (Finnish Red Cross permit 39/2016) by density centrifugation[28] and then labelled LDL with 1,1'-dioctadecyl-3,3,3',3'-tetramethyl-indocarbocyanine perchlorate (DiI) as described[29]. 4′,6-diamidino-2-phenylindole (DAPI), Poly-D lysine (PDL) and Histopacque Premium were obtained from Sigma. DiI, anti-mouse Alexa 568, HCS CellMask Deep Red and HCS CellMask Green were obtained from Thermo Fisher. Mouse anti-LDLR (clone 472413) was from R&D systems.

Peripheral blood mononuclear cells (PBMC) and blood samples: All blood samples were collected in accordance with the declaration of Helsinki regarding experiments involving humans. He-FH patients were identified in the Metabolic Syndrome in Men study (METSIM)[21] and blood samples obtained during patient follow-up. Two He-FH patients (Cys325Tyr and Ser580Phe) for which we obtained PBMC and EBV lymphoblast samples were described previously[30]. PBMC samples from the Finnish population survey, FINRISK 2012, and the donor

linked data (including genotypes) were obtained from THL Biobank (www.thl.fi/biobank) and used under the Biobank agreements no 2016_15, 2016_117 and 2018_15. The FINRISK 2012 study groups consisting of donors with elevated LDL-c levels (LDL > 5 mM, hLDL-c) and normal levels (LDL-c 2.0-2.5 mM, nLDL-c) were age, gender and BMI matched. The donors in neither of groups had cholesterol lowering medication by the time of sampling, and based on a food frequency questionnaire, did not receive an elevated proportion of energy intake as saturated or trans-fat. Buffy coat samples from healthy blood donors were obtained from the Finnish Red Cross (permit 392016). Three healthy volunteers donated blood samples on two consecutive days after overnight fasting, to assess the intraindividual variation of LDL uptake and lipid mobilization.

Cell culture: Control EBV lymphoblasts (GM14664) were obtained from Coriell Cell Repository and cultured in RPMI-1640 supplemented with 15% FBS, penicillin/streptomycin (100 U/ ml each) and 2 mM L-Glutamine. For continuous culturing of EBV lymphoblasts, $3x10^6$ cells were transferred to 5 ml of fresh medium once a week. Cells were cryopreserved in 70% PBMC medium (RPMI-1640, penicillin/streptomycin, 2 mM L-glutamine, 1 mM sodium pyruvate, and 1 mM HEPES), 20% FBS and 10% DMSO.

PBMC isolation: Blood or buffy coat samples were mixed 1:1 with phosphate buffered saline (PBS) including 2.5 mM EDTA (PBS-E). The blood mixture was gently layered over Histopacque Premium (1.0073, for mononuclear cells) and centrifuged 40 min at 400 g. The

PBMC cell layer was removed, transferred to a new 15 ml reaction tube and mixed with PBS-E. Cells were centrifuged at 400 g for 10 min and incubated in 2 ml of red blood cell lysis buffer for 1 min (155 mM NH_4Cl, 12 mM $NaHCO_3$, 0.1 mM EDTA). 10 ml of PBS-E was added and cells were pelleted and washed with PBS-E. Then cells were resuspended in 5 ml PBMC medium (RPMI-1640, penicillin/streptomycin, 2 mM L-glutamine, 1 mM sodium pyruvate, and 1 mM HEPES), counted, pelleted and resuspended in freezing medium (70% PBMC-medium, 20% FBS, 10 % DMSO) and cryopreserved in liquid nitrogen.

Cell treatments, DiI-LDL uptake, transfer to imaging plates and fixation: Cryopreserved EBV lymphoblasts or PBMCs were thawed in PBMC medium, and centrifuged at 400 g for 10 min. The cells were resuspended in PBMC medium and transferred to wells of a 96 well plate containing FBS (10% final concentration) or LPDS (5% final concentration) and incubated for 24 h. For DiI-LDL uptake experiments 30 µg/ml DiI-LDL was added for 1 h at 37°C. Subsequently, cells were transferred to conical 96 well plates and centrifuged at 400 g for 10 min. Using a robotic platform (Opentrons, New York, USA) medium was removed and cells were resuspended in PBMC medium. Cells were centrifuged, automatically resuspended in PBMC medium and transferred to PDL coated 384 well high-content imaging plates (Corning). After 30 min of incubation at 37°C cells were automatically fixed with 4% paraformaldehyde in 250 mM HEPES, 1 mM $CaCl_2$, 100 µM $MgCl_2$, pH 7.4 and washed with PBS. For lipid droplet and LDLR surface stainings, cells were directly transferred to PDL coated 384 well high-content plates, adhered, automatically fixed and washed with PBS.

Lipid droplet analyses: Cells were processed as described before[27] with the following changes: Fixed cell samples were automatically stained with 1 µg/ml LD540 (Princeton BioMolecular Research) and 5 µg/ml DAPI. 3D stacks of optical slices were acquired automatically either with a Nikon Eclipse Ti-E inverted microscope equipped with a 40 × Planfluor objective with NA 0.75 and 1.5 zoom; duplicate wells, each with six image fields per patient, or with a PerkinElmer Opera Phenix High Content Imaging system with a 63x water immersion objective, NA 1.15; duplicate wells, each with 14, 16 (two wells combined) or 24 (two wells combined) image fields. Image stacks were automatically deconvolved either with Huygens software (Scientific Volume Imaging, b.v.) or a custom-made Python tool based on the open-source tools PSF generator[31] and deconvolution lab[32]. Maximum intensity projections were made from the deconvolved image stacks with custom Python tools. These tools can be accessed via: https://github.com/lopaavol/Oputils. Automated quantification of lipid droplets was performed as described previously[33–35].

LDLR surface staining: All staining procedures were performed automatically. Fixed cells were quenched with 50 mM NH_4Cl for 15 min and washed twice with PBS. Cells were incubated with block solution (PBS, 1% BSA) for 10 min followed by staining with mouse anti-LDLR in block solution for 60 min. Cells were washed three times with PBS followed by incubation with secondary antibody solution (anti-mouse-Alexa 568, DAPI 5 µg/ml and HCS CellMask Green stain 0.25 µg/ml) for 45 min at room temperature. Cells were washed with PBS and 3D stacks of optical slices were acquired for DAPI (nuclei), CellMask Green (cytoplasm), Alexa 568 (LDLR surface) and Alexa 640 (background) channels using an Opera Phenix high-content imaging

system with a 40x water immersion objective NA 1.1; quadruplicate wells, each with seven image fields per patient. LDLR surface and background images were automatically deconvolved with our custom build Python deconvolution tools and maximum intensity projections were made. The resulting images were automatically analysed with CellProfiler[36]. LDLR surface intensities were background subtracted for each individual cell and normalized by subtracting mean LDLR surface intensities from the two controls, which were included in each imaging plate.

Quantification of DiI-LDL uptake: DiI-LDL labeled, and fixed cells (see section cell treatments) were automatically processed with a robotic platform (Opentrons). Cells were stained with 5 µg/ml DAPI and 0.5 µg/ml HCS CellMask Deep Red and image stacks for three channels, DAPI (nuclei), DiI-LDL and CellMask Deep Red (cytoplasm) were acquired. Automated microscopy and single cell quantifications with CellProfiler were performed as described in the section LDLR surface staining; Quadruplicate wells, each with 7 image fields for heterozygous FH patients; duplicate wells, each with 13 image fields for FINRISK subjects. Plate effects were determined with control samples and corrected for in the individual experiments.

LDL polygenic risk score (LDL-PRS)*:* We calculated the LDL PRS using the LDpred method based on both the previously published PRS by *Talmud* et al. and a European genome-wide association study (GWAS) meta-analysis with 56945 samples[4,37]. The PRS calculation is described in greater detail in the supplementary methods section. LDL uptake and lipid

mobilization parameters were normalized to a range from 0 to 1 to generate uptake and mobilization scores. Hybrid scores represent the average of LDL-PRS and uptake and/or mobilization scores which were normalized to a range from 0 to 1.

Data analysis: Lymphocytes and monocytes were detected based on the size of the cytoplasm (Ly <115 μm^2, Mo >115 μm^2) (See **Extended Data Fig. 1**). We averaged the cellular mean DiI-LDL intensities and organelle counts for each cell population and well and normalized them to the average of both controls included in each plate, set to 100%. For LD quantifications we first selected monocytes with at least one LD. We then averaged cellular LD number and total LD area (LD number x LD size) for each well. For lipid mobilization we first averaged the control medium results for LD-Pos, LD-No, and LD-area from duplicate wells and then divided these by the respective per well results after lipid starvation. We used Python (Python Software Foundation, www.python.org) with the following packages to perform the single cell data analysis (Pandas, Numpy, Scipy, Matplotlib[38], Seaborn[39]). For statistical significance testing we first performed Levene's test to assess the equality of sample variation. For equal sample amounts and variance, we performed two-tailed Student's t-test. For unequal samples or variance, we utilized Welch's t-test. For correlations we first performed a linear regression of the two measurements and then calculated a two-sided p-value for a hypothesis test whose null hypothesis is that the slope is zero, using Wald Test with t-distribution of the test statistic. Fisher's exact probability test was used to calculate the odds ratio.

Acknowledgements:

We thank Anna Uro for technical assistance; HiLIFE and Biocenter Finland supported Helsinki BioImaging infrastructures for help with microscopy; Katariina Öörni for help with LDL preparation; Abel Szkalisity for help with image analysis. We thank THL Biobank for providing samples and data for this study (study no: 2016_15, 2016_117 and 2018_15) and all biobank donors for their participation in biobank research. This study was supported by The Academy of Finland (grants 282192, 284667, 307415 to E.I.; 321428 to M.L.; 310552 to LP; 328861, 325040 to SP; and 312062, 316820 to SR), Sigrid Juselius Foundation (grant to E.I. M.L. S.R.), University of Helsinki (grant to K.K.; Faculty of Medicine early-career investigator grant to SP; HiLIFE Fellow grant to E.I.), Finnish Foundation for Cardiovascular Research and University of Helsinki HiLIFE Fellow and Grand Challenge grants, and H2020-INTERVENE (101016775) to SR, MIUR of Italy (project cod. PON03PE_00060_7, grant to CEINGE, G.F.), LENDULET-BIOMAG Grant (2018-342), H2020-discovAIR (874656), and Chan Zuckerberg Initiative (seed networks for the HCA-DVP) to PH. Ida Montin Foundation (grant to P.R.), Doctoral Programme in Population Health, University of Helsinki (grant to P.R.); Emil Aaltonen Foundation (grant to P.R.)

Author contributions:

S.G.P and E.I. designed the study and developed the concept. S.G.P, I.B., K.K., I.H., and P.R. performed experiments. S.G.P, I.B., K.K. I.H., P.R., M.M.I., S.R. and E.I. analyzed data and interpreted results, A.K., M.D.T., A.S.F., G.F., J.K. and M.L. provided patient samples and

clinical data. L.P. and P.H. established image analysis and processing tools. S.G.P and E.I. wrote the manuscript. All authors reviewed and revised the manuscript.

Competing interests:

A patent application covering the use of the here suggested patient stratification methods has been filed (Application: FI 20206284) in which University of Helsinki is the applicant and EI and SP are the inventors.

References:

1. Borén, J. *et al.* Low-density lipoproteins cause atherosclerotic cardiovascular disease: pathophysiological, genetic, and therapeutic insights: a consensus statement from the European Atherosclerosis Society Consensus Panel. *Eur. Heart J.* (2020) doi:10.1093/eurheartj/ehz962.
2. Abul-Husn, N. S. *et al.* Genetic identification of familial hypercholesterolemia within a single U.S. health care system. *Science* **354**, aaf7000 (2016).
3. Khera, A. V. *et al.* Diagnostic Yield and Clinical Utility of Sequencing Familial Hypercholesterolemia Genes in Patients With Severe Hypercholesterolemia. *Journal of the American College of Cardiology* **67**, 2578–2589 (2016).
4. Talmud, P. J. *et al.* Use of low-density lipoprotein cholesterol gene score to distinguish patients with polygenic and monogenic familial hypercholesterolaemia: a case-control study. *The Lancet* **381**, 1293–1301 (2013).
5. Ripatti Pietari *et al.* Polygenic Hyperlipidemias and Coronary Artery Disease Risk. *Circulation: Genomic and Precision Medicine* **13**, e002725 (2020).
6. Mach, F. *et al.* 2019 ESC/EAS guidelines for the management of dyslipidaemias: Lipid modification to reduce cardiovascular risk. *Atherosclerosis* **290**, 140–205 (2019).
7. Ridker, P. M., Mora, S. & Rose, L. Percent reduction in LDL cholesterol following high-intensity statin therapy: potential implications for guidelines and for the prescription of emerging lipid-lowering agents. *Eur Heart J* **37**, 1373–1379 (2016).
8. Boekholdt, S. M. *et al.* Very Low Levels of Atherogenic Lipoproteins and the Risk for Cardiovascular Events: A Meta-Analysis of Statin Trials. *Journal of the American College of Cardiology* **64**, 485–494 (2014).
9. Ballantyne, C. M. Achieving greater reductions in cardiovascular risk: lessons from statin therapy on risk measures and risk reduction. *American Heart Journal* **148**, S3–S8 (2004).

10. Snijder, B. *et al.* Image-based ex-vivo drug screening for patients with aggressive haematological malignancies: interim results from a single-arm, open-label, pilot study. *Lancet Haematol* **4**, e595–e606 (2017).

11. Hagemenas F C & Illingworth D R. Cholesterol homeostasis in mononuclear leukocytes from patients with familial hypercholesterolemia treated with lovastatin. *Arteriosclerosis: An Official Journal of the American Heart Association, Inc.* **9**, 355–361 (1989).

12. Gaddi, A. *et al.* Pravastatin in heterozygous familial hypercholesterolemia: Low-density lipoprotein (LDL) cholesterol-lowering effect and LDL receptor activity on skin fibroblasts. *Metabolism* **40**, 1074–1078 (1991).

13. Raungaard, B., Brorholt Petersen, J. U., Jensen, H. K. & Færgeman, O. Flow Cytometric Assessment of Effects of Fluvastatin on Low-Density Lipoprotein Receptor Activity in Stimulated T-Lymphocytes from Patients with Heterozygous Familial Hypercholesterolemia. *The Journal of Clinical Pharmacology* **40**, 421–429 (2000).

14. Chan, P., Jones, C., Lafrenière, R. & Parsons, H. G. Surface expression of low density lipoprotein receptor in EBV-transformed lymphocytes: characterization and use for studying familial hypercholesterolemia. *Atherosclerosis* **131**, 149–160 (1997).

15. Schmitz G, Brüning T, Kovacs E & Barlage S. Fluorescence flow cytometry of human leukocytes in the detection of LDL receptor defects in the differential diagnosis of hypercholesterolemia. *Arteriosclerosis and Thrombosis: A Journal of Vascular Biology* **13**, 1053–1065 (1993).

16. Piccaluga, P. P., Weber, A., Ambrosio, M. R., Ahmed, Y. & Leoncini, L. Epstein–Barr Virus-Induced Metabolic Rearrangements in Human B-Cell Lymphomas. *Front Microbiol* **9**, (2018).

17. Romano, M. *et al.* Identification and functional characterization of LDLR mutations in familial hypercholesterolemia patients from Southern Italy. *Atherosclerosis* **210**, 493–496 (2010).

18. Benito-Vicente, A. *et al.* Validation of LDLr Activity as a Tool to Improve Genetic Diagnosis of Familial Hypercholesterolemia: A Retrospective on Functional Characterization of LDLr Variants. *International Journal of Molecular Sciences* **19**, 1676 (2018).

19. Ikonen, E. Cellular cholesterol trafficking and compartmentalization. *Nat. Rev. Mol. Cell Biol.* **9**, 125–138 (2008).

20. Luo, J., Yang, H. & Song, B.-L. Mechanisms and regulation of cholesterol homeostasis. *Nat Rev Mol Cell Biol* **21**, 225–245 (2020).

21. Laakso, M. *et al.* The Metabolic Syndrome in Men study: a resource for studies of metabolic and cardiovascular diseases. *J. Lipid Res.* **58**, 481–493 (2017).

22. Lahtinen, A. M., Havulinna, A. S., Jula, A., Salomaa, V. & Kontula, K. Prevalence and clinical correlates of familial hypercholesterolemia founder mutations in the general population. *Atherosclerosis* **238**, 64–69 (2015).

23. Borodulin, K. *et al.* Cohort Profile: The National FINRISK Study. *Int J Epidemiol* **47**, 696–696i (2018).

24. Klop, B., Elte, J. W. F. & Cabezas, M. C. Dyslipidemia in obesity: mechanisms and potential targets. *Nutrients* **5**, 1218–1240 (2013).

25. Mamo, J. C. L. *et al.* Postprandial dyslipidemia in men with visceral obesity: an effect of reduced LDL receptor expression? *American Journal of Physiology-Endocrinology and Metabolism* **281**, E626–E632 (2001).

26. Wiegman, A. *et al.* Familial hypercholesterolaemia in children and adolescents: gaining decades of life by optimizing detection and treatment. *Eur Heart J* **36**, 2425–2437 (2015).

27. Goldstein, J. L., Basu, S. K. & Brown, M. S. Receptor-mediated endocytosis of low-density lipoprotein in cultured cells. *Meth. Enzymol.* **98**, 241–260 (1983).

28. Stephan, Z. F. & Yurachek, E. C. Rapid fluorometric assay of LDL receptor activity by DiI-labeled LDL. *J. Lipid Res.* **34**, 325–330 (1993).

29. Reynolds, G. D. & St Clair, R. W. A comparative microscopic and biochemical study of the uptake of fluorescent and 125I-labeled lipoproteins by skin fibroblasts, smooth muscle cells, and peritoneal macrophages in culture. *Am J Pathol* **121**, 200–211 (1985).

30. Romano, M. *et al.* An improved method on stimulated T-lymphocytes to functionally characterize novel and known LDLR mutations. *J Lipid Res* **52**, 2095–2100 (2011).

31. Kirshner, H., Aguet, F., Sage, D. & Unser, M. 3-D PSF fitting for fluorescence microscopy: implementation and localization application. *Journal of Microscopy* **249**, 13–25 (2013).

32. Sage, D. *et al.* DeconvolutionLab2: An open-source software for deconvolution microscopy. *Methods* **115**, 28–41 (2017).

33. Pfisterer, S. G. *et al.* Role for formin-like 1-dependent acto-myosin assembly in lipid droplet dynamics and lipid storage. *Nature Communications* **8**, 14858 (2017).

34. Vanharanta, L. *et al.* High-content imaging and structure-based predictions reveal functional differences between Niemann-Pick C1 variants. *Traffic* **21**, 386–397 (2020).

35. Salo, V. T. *et al.* Seipin Facilitates Triglyceride Flow to Lipid Droplet and Counteracts Droplet Ripening via Endoplasmic Reticulum Contact. *Developmental Cell* **50**, 478-493.e9 (2019).

36. Carpenter, A. E. *et al.* CellProfiler: image analysis software for identifying and quantifying cell phenotypes. *Genome Biology* **7**, R100 (2006).

37. Vilhjálmsson, B. J. *et al.* Modeling Linkage Disequilibrium Increases Accuracy of Polygenic Risk Scores. *Am. J. Hum. Genet.* **97**, 576–592 (2015).

38. Hunter, J. D. Matplotlib: A 2D Graphics Environment. *Computing in Science Engineering* **9**, 90–95 (2007).

39. Michael Waskom *et al. mwaskom/seaborn: v0.8.1 (September 2017)*. (Zenodo, 2017). doi:10.5281/zenodo.883859.

Figure legends:

Figure 1: Automated analysis pipeline for multiplex quantification of functional phenotypes in PBMCs. a) Schematic presentation of the automated analysis pipeline. For each experiment cryopreserved PBMC samples were thawed, aliquoted into 96 wells and incubated overnight with lipid rich (CM, 10% FBS) or lipid poor medium (LP, 5% LPDS). Cells were labeled with fluorescent LDL (DiI-LDL) or directly transferred to 384 well imaging plates, automatically fixed, stained and subjected to automated high-content imaging. Images were quantified with CellProfiler and single-cell data was processed with Python tools. **b**) Representative images of lymphocyte and monocyte DiI-LDL uptake after lipid starvation. **c**) Histogram for cellular DiI-LDL intensities in lymphocytes and monocytes (**d**) from a single well. **e**) Quantification of mean DiI-LDL intensities and DiI-LDL organelles (**f**) in lymphocytes (Ly) and monocytes (Mo); representative of eight independent experiments, each with four wells per treatment; Student's t-test. **g**) Representative images of DiI-LDL uptake in monocytes isolated from FH patients with *LDLR* mutations Cys325Tyr or Ser580Phe and a control after lipid starvation. **h**) Quantification of monocyte (Mo) and lymphocyte (Ly) cellular DiI-LDL intensities (Int), DiI-LDL organelle numbers (No) and pan-uptake; duplicate wells / patient (eight wells / patient for pan-uptake). Significant changes to control 2 were calculated with Welch's t-test. ***$p < 0.001$, **$p < 0.01$, scale bar = 10 µm, error bars = SEM.

Figure 2) Heterogeneous LDL uptake and LDLR surface expression in He-FH patients' monocytes. a) Schematic presentation of *LDLR* mutations included in this study together with their pathogenicity status from ClinVar and LOVD databases. (P = pathogenic, LP = likely

pathogenic, LB = likely benign, VUS = variant of unknown significance. **b**) Quantification of monocyte (Mo) and lymphocyte (Ly) cellular DiI-LDL intensities (Int), organelle numbers (No) and pan-uptake normalized to two controls (100%); two to three independent experiments, each with duplicate or quadruplicate wells per patient (8-16 wells per patient for pan-uptake), Cys325Tyr and Ser580Phe were described in (**Fig. 1g, h**). Significant changes to control two were calculated with Welch's t-test. **c**) Correlation of pan-uptake and monocyte LDLR surface expression, including R- and p-values for all uptake scores; n = 21 patients. **d**) Correlation of monocyte DiI-LDL intensities with circulating LDL-cholesterol (LDL-c) for heterozygous FH patients on statin monotherapy, including R- and p-values for all uptake scores. **e**) LDL-c concentration for good (white) and poor (purple) statin responders defined as 30% of patients with the highest and lowest monocyte mean DiI-LDL intensity as in **d**. Grey areas in scatter plots indicate 95% CI, *p<0.05, ** p<0.01, *** p<0.001.

Figure 3) LDL uptake profiles in non-FH individuals with normal and elevated LDL-c. a) Quantification of monocyte (Mo) and lymphocyte (Ly) mean DiI-LDL intensities (Int), organelle numbers (No) and pan-uptake after lipid starvation, normalized to control standards; duplicate wells per patient (eight wells per patient for pan-uptake). Significant changes to control two were calculated with Welch's t-test. **b**) Correlation of pan-uptake with waist circumference and **c**) with body mass index (BMI), including R- and p-values for all uptake scores. n = 39. Grey areas in scatter plots indicate 95% CI. *p<0.05, ** p<0.01, *** p<0.001.

Figure 4) Lipid mobilization assay. a) Representative images showing lipid droplets (LDs) in lymphocyte and monocyte populations after treatment with control medium, scale bar = 10µm. **b**) Histogram for cellular LD counts in lymphocyte and (**c**) monocyte populations after treatment with control medium (CM) and lipid starvation (LP) from a single well. **d**) Quantification of LD positive cells in lymphocytes (Ly) and monocytes (Mo) upon treatment with control medium (CM) and lipid starvation (LP); representative of three independent experiments, each with duplicate wells per patient and treatment. **e**) LD counts and (**f**) total LD area in LD positive monocytes quantified for the same experiment as in (**d**). **g**) Schematic presentation of the lipid mobilization score. Upon lipid starvation, the fraction of LD positive monocytes (LD-Pos), their total LD area (LD-Area) and LD numbers (LD-No) are decreasing. Mobilization scores are calculated by dividing the amount of LD-Pos, LD-No or LD-Area in CM with the respective quantifications after lipid starvation. Pan-mobilization is the average of LD-Pos, LD-No and LD-Area mobilization scores from individual wells. **h**) Lipid mobilization scores for one control; n = 6 wells from three independent experiments, (18 wells for pan-mobilization), ± SEM. **i**) Pan-mobilization for controls (combined control one and two from five experiments), FH-North-Karelia (n = 7), FH-Pogosta (n = 3) and FH-Glu626 (n = 5). **j**) Correlation of combined monocyte mean DiI-LDL intensities and pan-mobilization with circulating LDL-c. **k**) LDL-c concentration for good (white) and poor (purple) statin responders defined as 30% of patients with the highest and lowest combined score as in **j**. *$p < 0.05$, **$p < 0.01$

Figure 5) Monocyte lipid mobilization correlates with LDL uptake and is reduced in subjects with elevated LDL-c. a) Mobilization scores (Pos, LD-No, LD-Area and pan-

mobilization) in monocytes from controls (nLDLc, LDL-c 2-2.5 mmol/l) and individuals with elevated LDL-c (hLDL-c, LDL > 5 mmol/l) sorted according to the pan-uptake score (**Fig. 3a**); duplicate wells per patient (six wells per patient for pan-mobilization). Significant changes to control two were quantified with Welch's t-test. **b**) Box plot of pan-mobilization for nLDL-c and hLDL-c subgroups; nLDL-c n = 19, hLDL-c n = 19. ** $p < 0.01$, Students t-test. Correlation of pan-mobilization with pan-uptake (**c**), BMI (**d**) and age (**e**) including R- and p-values for all mobilization scores. Grey areas in scatter plots = 95% CI. * $p<0.05$, * $p<0.01$, *$p<0.001$.

Figure 6) Hybrid scores combining genetic and functional cell based data to improve risk assessment in hypercholesterolemia. a) Box plot of a polygenic risk score for high LDL-c levels (LDL-PRS) for nLDL-c (2-2.5 mmol/l LDL-c) and hLDL-c (>5 mmol/l LDL-c) subgroups. **b**) Box plot for double hybrid scores combining LDL-PRS and pan-uptake or pan-mobilization (**c**) into a single score. **d**) Box plot for a triple hybrid score consisting of LDL-PRS, pan-uptake and mobilization. nLDL-c n = 18, hLDL-c n = 19, * $p<0.05$, ** $p<0.01$, *** $p<0.001$; Welch's t-test. **e**) Odds ratio (OR) for 30% of the individuals with the highest LDL-PRS, double or triple hybrid scores and the remaining subjects, calculated with the Fisher's exact probability test.

Graphical abstract) Schematic illustration of functional readouts in peripheral blood mononuclear cells and their correlation with physiological outcomes in monogenic and polygenic hypercholesterolemia.

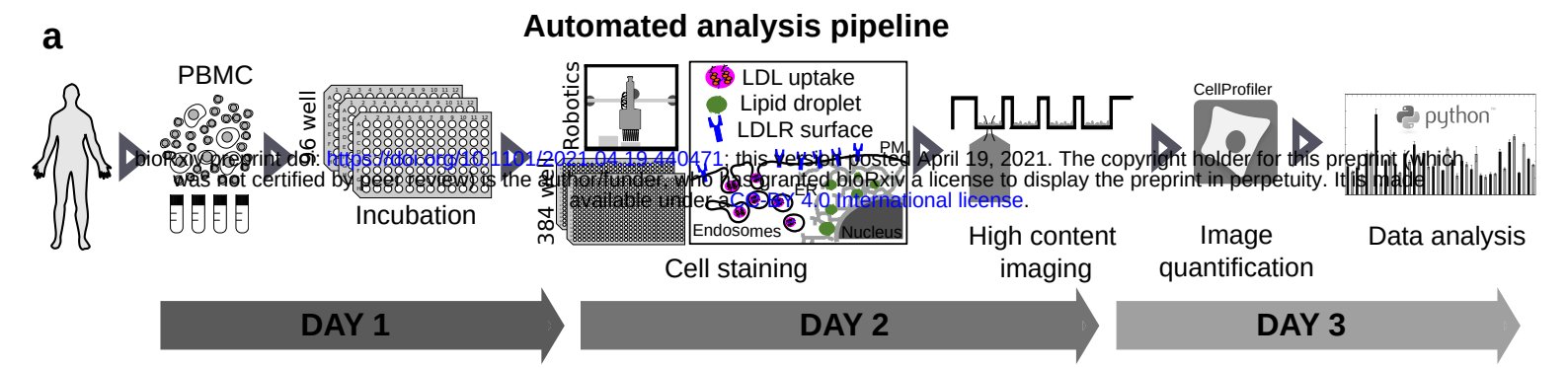

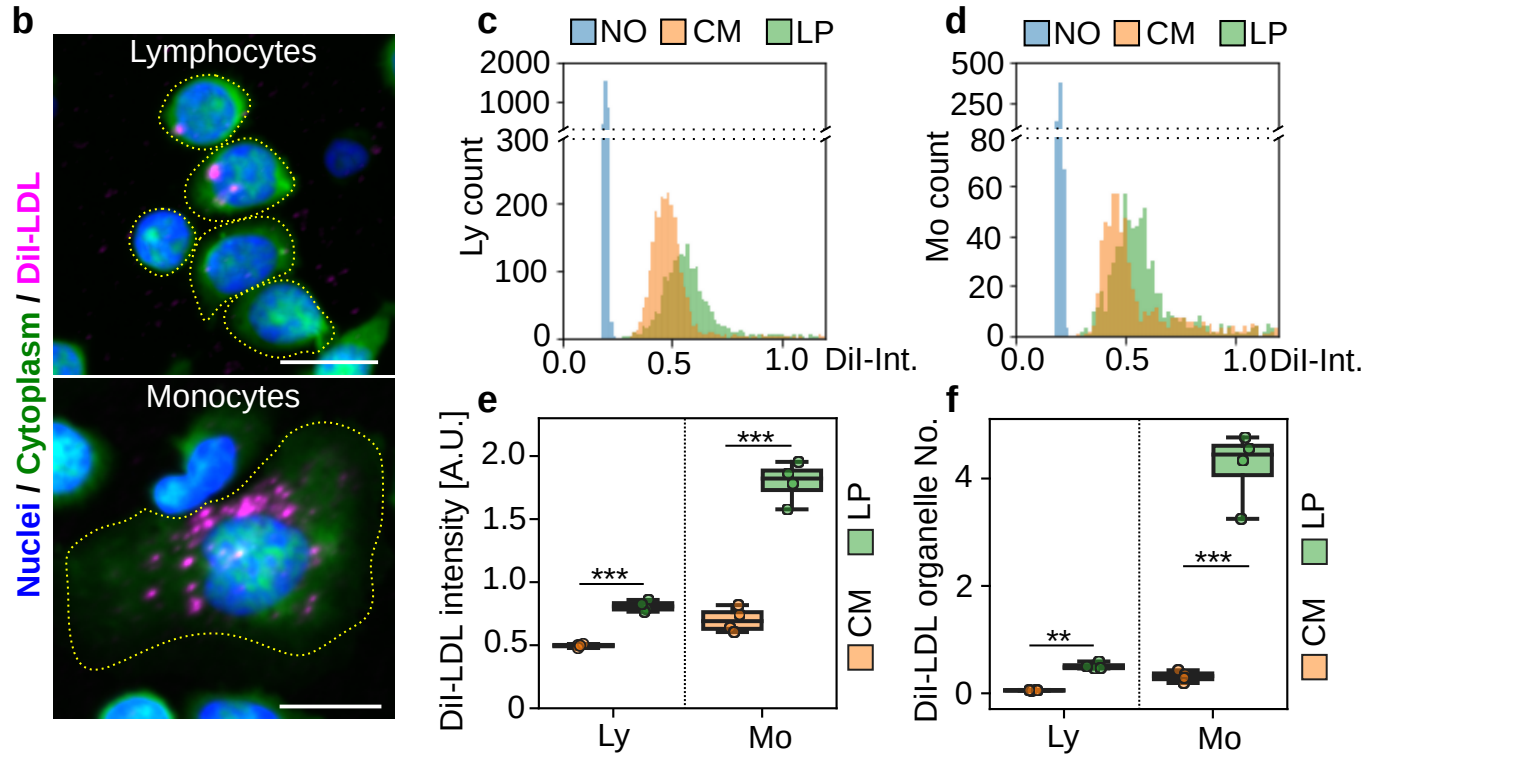

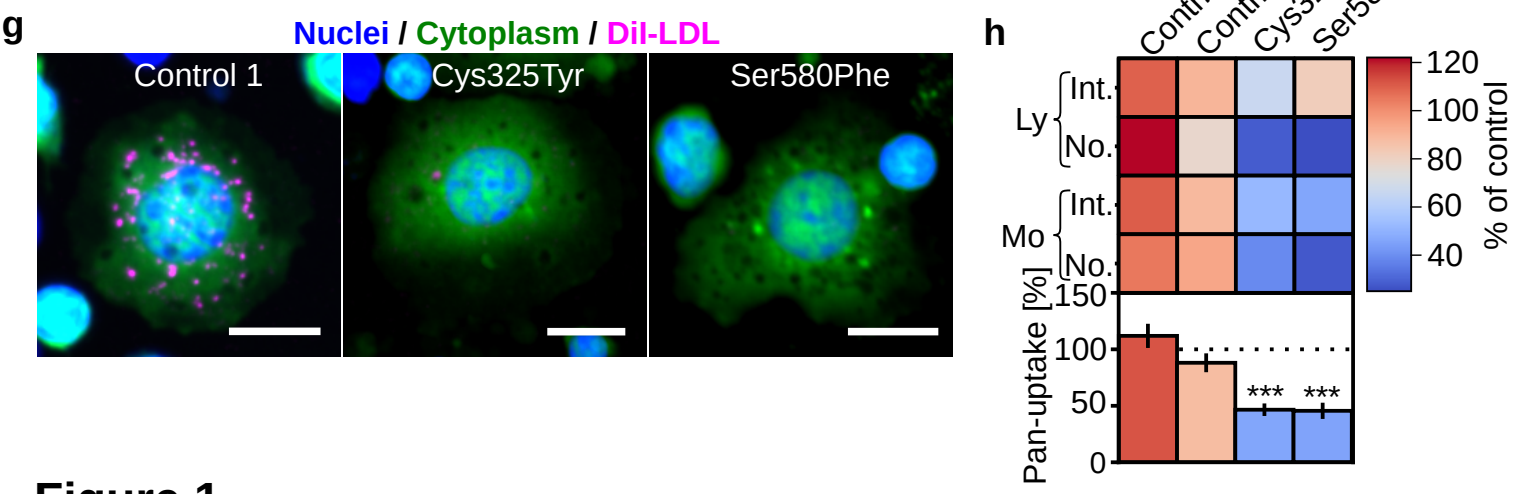

Figure 1

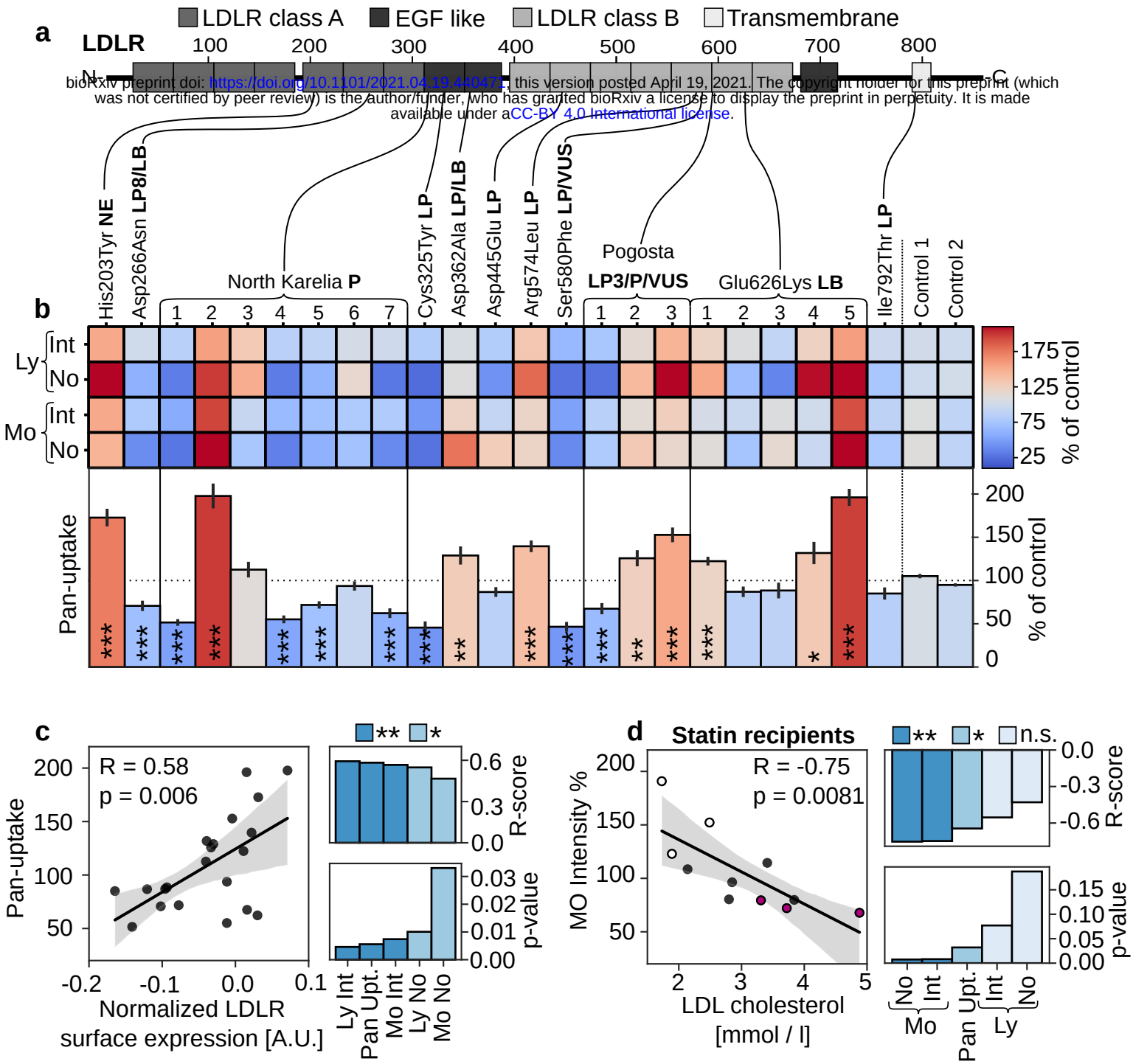

Figure 2

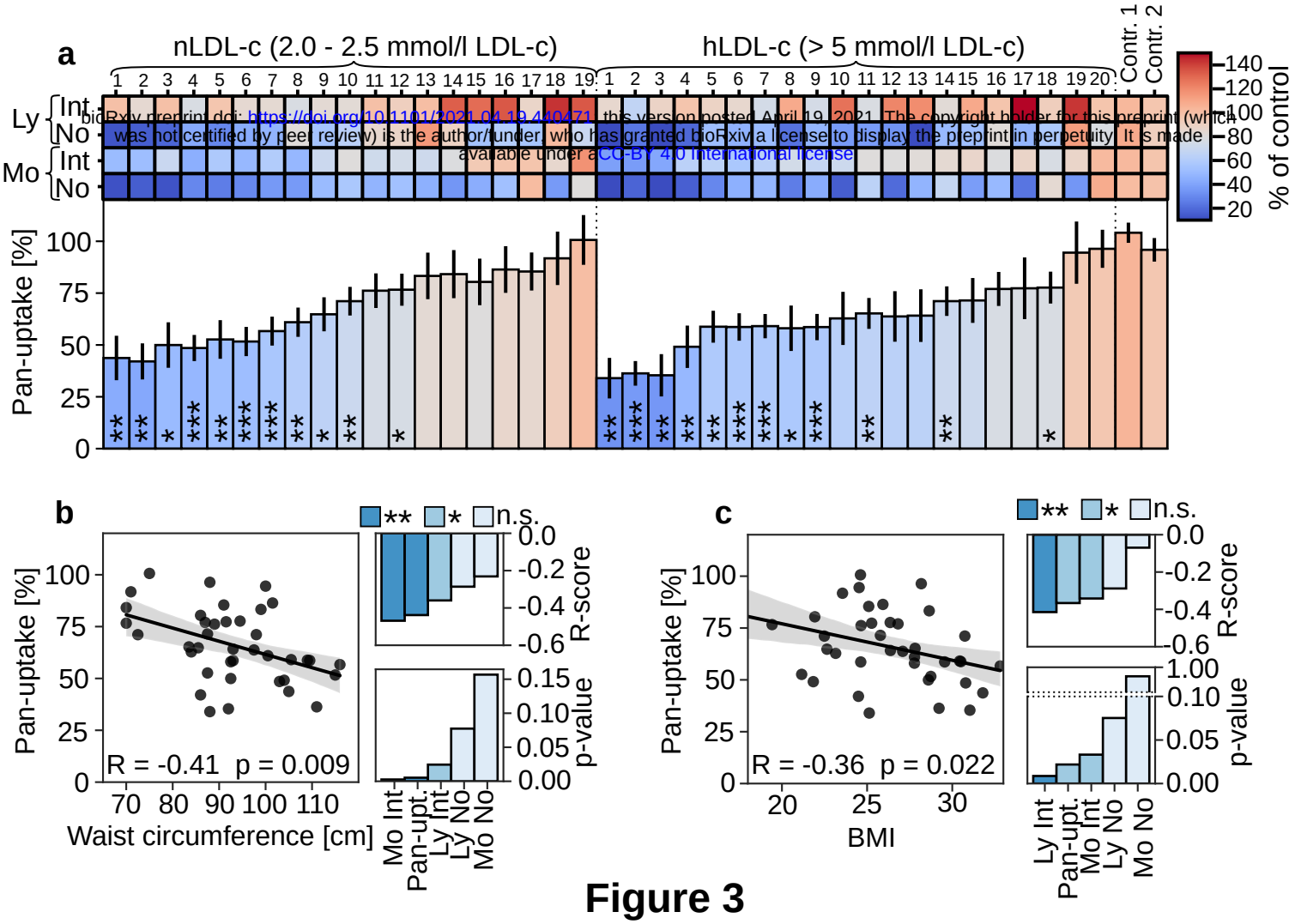

Figure 3

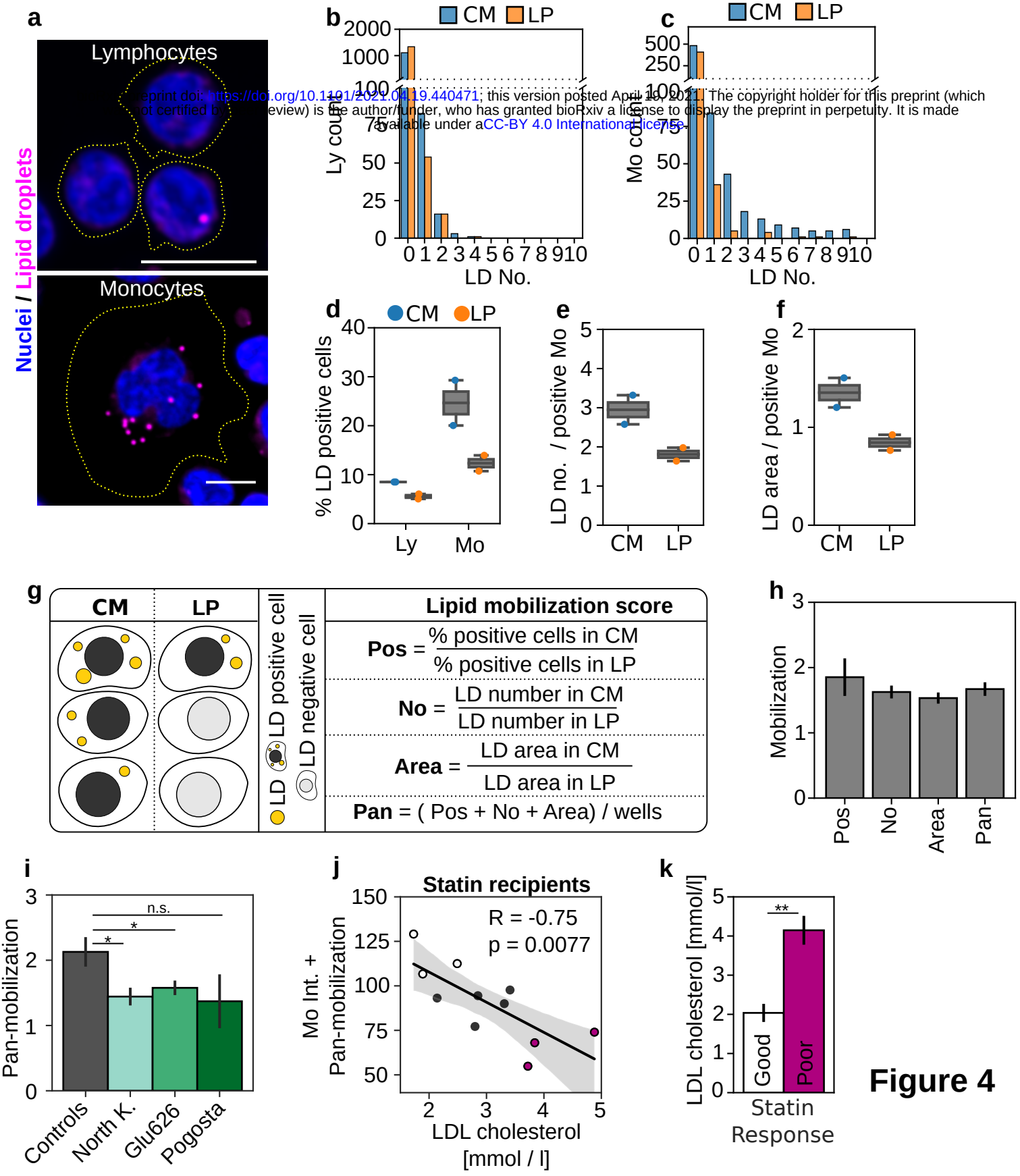

Figure 4

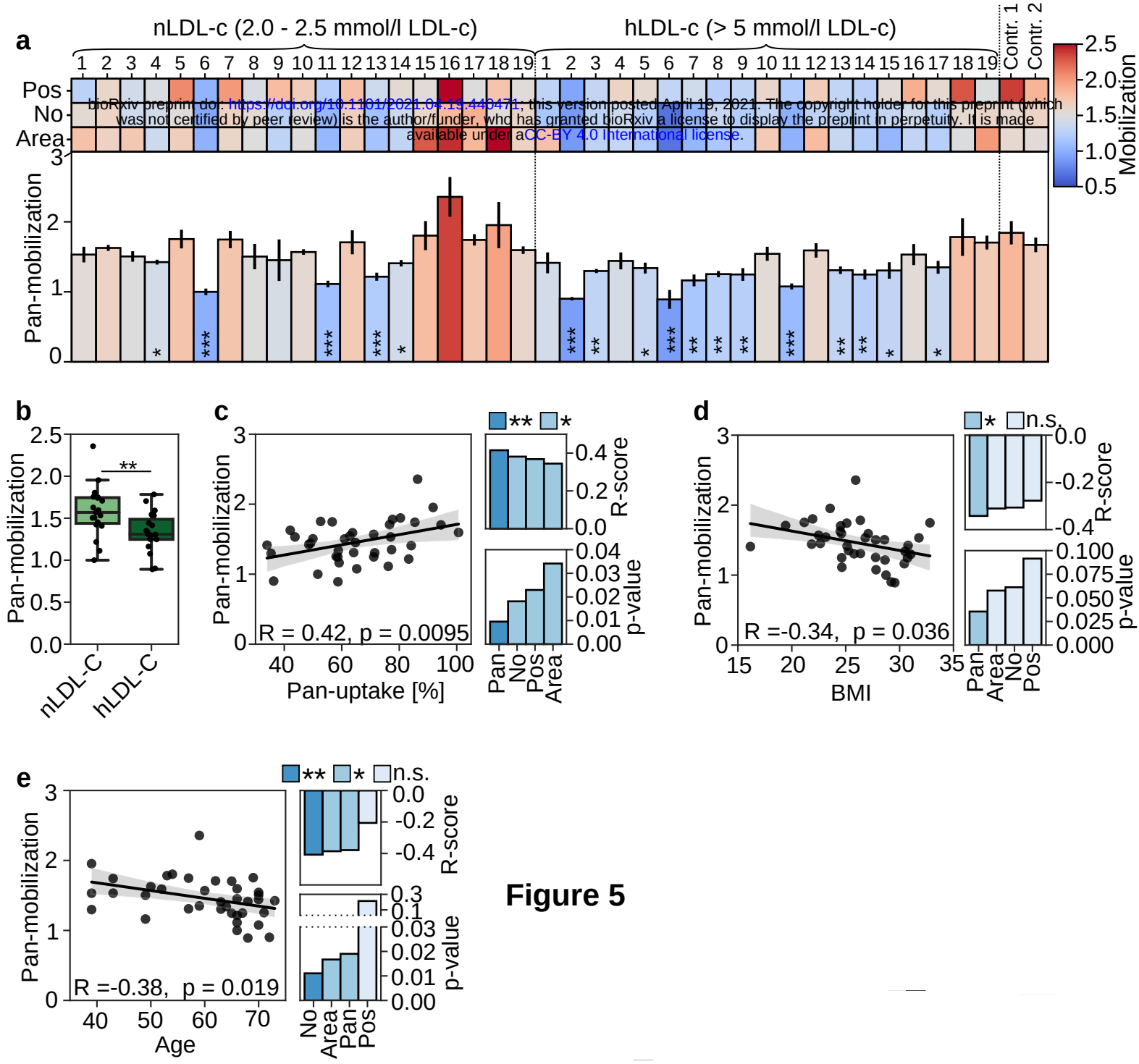

Figure 5

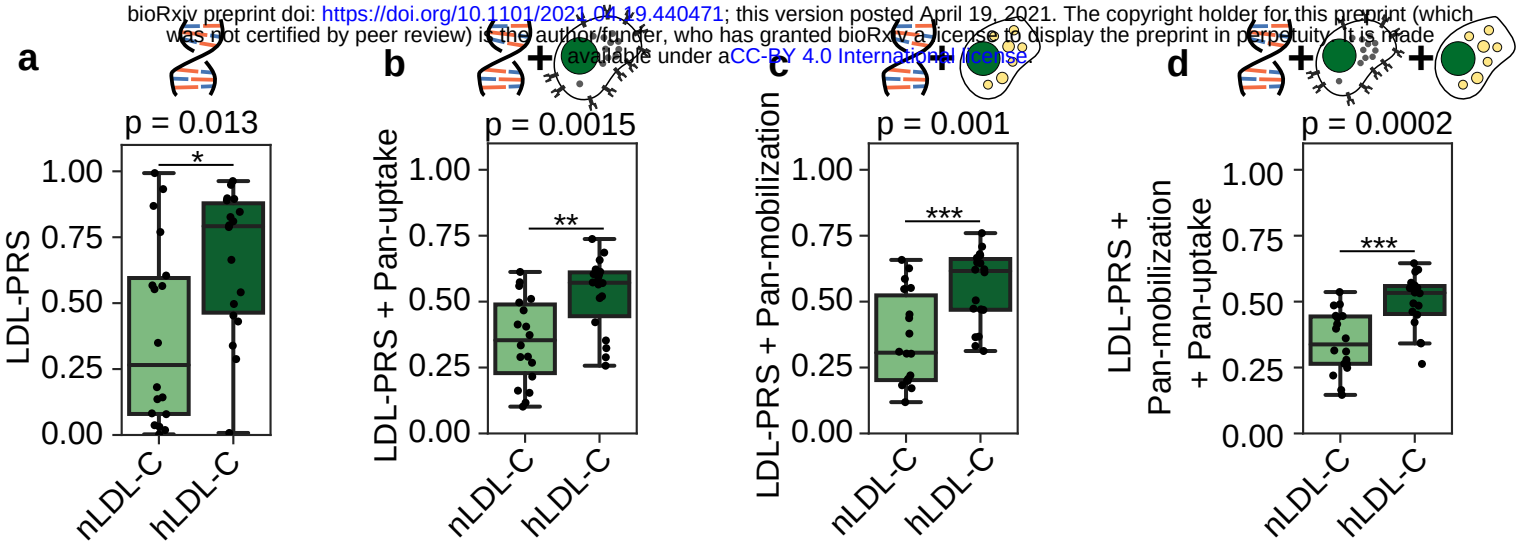

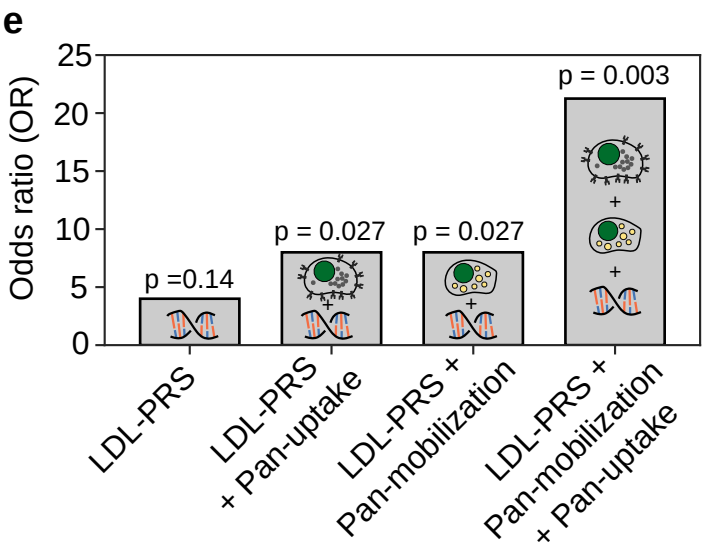

Figure 6)

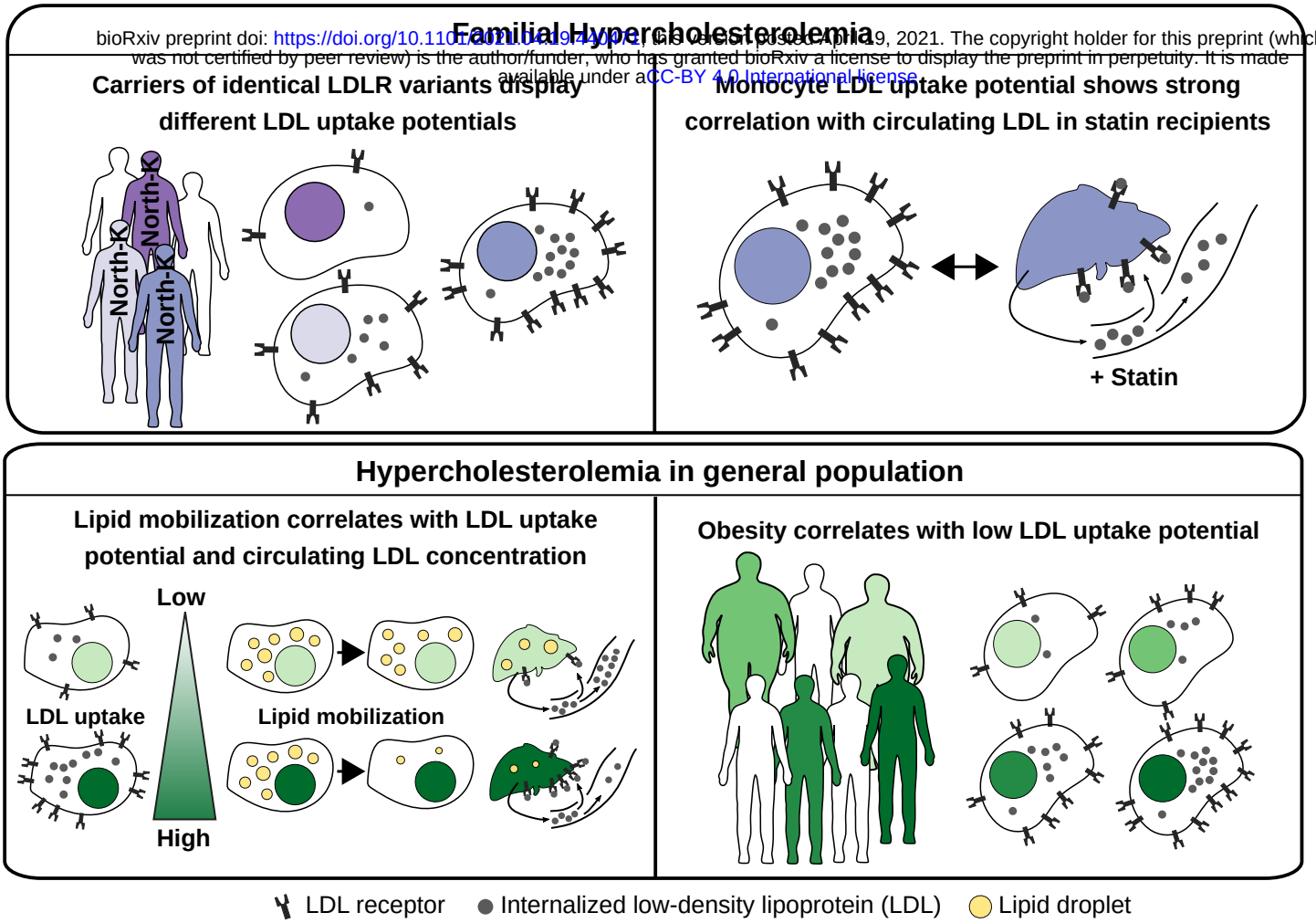

Graphical abstract